

Analysis and Comparison of Morphological Reconstructions of Hippocampal Field CA1 Pyramidal Cells

José Ambros-Ingerson* and William R. Holmes

ABSTRACT: Morphological reconstructions have become a routine and valuable tool for neuroscientists. The accuracy of reconstructions is a matter of considerable interest given that they are widely used in computational studies of neural function. Despite their wide usage, comparisons of reconstructions obtained using various methodologies are lacking. We reviewed reconstructions of hippocampal CA1 pyramidal cells from five published studies and found marked differences in some of the most basic measurements. For four of the five studies means of total cell length clustered in the 11,479–13,417- μm range. The remaining study had a significantly larger value for this index at $16,992 \pm 5,788 \mu\text{m}$. Surface area means varied more than 4-fold from 16,074 to 67,102 μm^2 . Volume means varied more than 8-fold from 3,828 to 30,384 μm^3 . Simulated passive input resistance means varied from 38.0 to 172.1 M Ω , reflecting the variability in cell dimensions. Estimates of the electrotonic length varied from 1.26 to 1.56. In two reconstructions used in previously published studies, simulated somatic excitatory postsynaptic potentials (EPSPs) varied 2–4-fold in amplitude, time to peak and half-width, for synaptic inputs at similar locations. Substantial jitter on the z-axis was identified as one likely source of the discrepancy in total cell length, while substantial differences in diameter measurements across studies, and sometimes within the same study, accounted for the variability in surface area and volume. While some part of the observed variability is surely due to the diversity of CA1 pyramidal cells, our analysis suggests that a substantial portion stemmed from methodological inconsistencies and from technological limitations. Suggestions are made for improving the quality and usefulness of morphological reconstructions. We conclude that reconstructions across studies have substantial variability in measures that are very relevant to neuronal function. Consequently, modelers are advised to use more than just one reconstructed cell in their simulations of neural function. © 2004 Wiley-Liss, Inc.

KEY WORDS: hippocampus; biophysics; electrophysiology; neurophysiology; computer models

INTRODUCTION

Morphological reconstructions have become a very important and valuable tool in attempts to understand neural function. The availability of detailed reconstructions has made possible the study of the physiology of neurons by means of computational studies based on real neurons. In particular, morphological reconstructions of CA1 pyramidal cells are now routinely used in computer simulations in both theoretical and experimental

neurophysiology studies. This has been made possible by anatomists who, in the best scientific sharing spirit, made the products of their hard work available to the computational neuroscience community.

Data from morphological reconstructions often form the backbone of computer simulations onto which additional features or processes, like membrane channels, are attached. Results from these simulations have provided numerous insights. They have been used, for example, to make explicit a theory's assumptions and mechanisms (Kager et al., 2002), quantify in detail electrophysiological variables (Mainen et al., 1996; Jaffe and Carnevale, 1999), render quantitative assessments of proposed hypotheses (Nasuto et al., 2001; Desjardins et al., 2003; Watanabe et al., 2002; Magee and Cook, 2000), integrate the experimental results from diverse fields of study (Poirazi et al., 2003), articulate predictions (Migliore, 2003), and suggest directions for further research (Migliore, 1996; Migliore et al., 1999; Poolos et al., 2002). Reliance on simulation results has increased as models grow in sophistication, and the complexity of the phenomena under study overwhelms unassisted reasoning.

Because assessments of neuronal function are based on reconstruction measurements and neuron reconstructions are increasingly being used in computational studies, the accuracy of these reconstructions is of considerable interest. The physiological relevance of simulation results critically depends on the accuracy of the reconstructions they use. Methods of neuronal reconstruction are varied, and there is no clear consensus about the most accurate method to use. Despite their wide usage, comparisons of reconstructions obtained using various methodologies are lacking.

We analyzed reconstructions of pyramidal cells from field CA1 in hippocampus from five published studies. We compared basic cell measurements across these studies, including total length, surface area, and volume, as these indices play key roles in the electrophysiological behavior of individual neurons (Rall, 1977), and are vitally important for assessing neural function. While there was agreement in four of five studies in total cell length, there were wide discrepancies in the surface area and volume indices. As would be expected from the above results, we found large variations in input resistance (R_N) and excitatory postsynaptic potential (EPSP) shape indices when computing these measures in simulations under passive membrane conditions.

Department of Biological Sciences, Neuroscience Program, Ohio University, Athens, Ohio

Grant sponsor: NIAAA; Grant number: AA014294-01.

*Correspondence to: José Ambros-Ingerson, Department of Biological Sciences, Irvine Hall, Ohio University, Athens OH 45701.

E-mail: ambros@alumni.uci.edu

Accepted for publication 10 August 2004

DOI 10.1002/hipo.20051

Published online 15 October 2004 in Wiley InterScience (www.interscience.wiley.com).

While a portion of the observed variability surely reflects biological diversity of CA1 pyramidal cells, our results suggest that a substantial portion is due to methodological issues. We have identified likely methodological and technological sources of variability through a detailed analysis of the results. We conclude with a list of suggestions that we believe would improve the quality and usefulness of future reconstructions and would improve the robustness of simulation results that use reconstructions.

A brief description of some of the results presented in this article has appeared in abstract form (Ambros-Ingerson and Holmes, 2003).

MATERIALS AND METHODS

We used Medline to search the scientific literature for publications that reported morphological reconstructions of hippocampal field CA1 pyramidal cells. We found five studies, (Bannister and Larkman, 1995; Carnevale et al., 1997; Ishizuka et al., 1995; Megias et al., 2001; Pyapali et al., 1998) which we refer to as BAN, CAR, ISH, MEG, and PYA, respectively, hereafter.

We located digital reconstructions for three of the studies through a web search. Cells from the CAR study (Carnevale et al., 1997) were downloaded from Brenda Clairborne's web site (<http://www.utsa.edu/clairbornelab>), those for the MEG study (Megias et al., 2001) were downloaded from Attila Gulyás' website (<http://www.koki.hu/~gulyas/calcells>) and those for the PYA study (Pyapali et al., 1998) were downloaded from the Duke/Southampton Archive of Neuronal Morphology website (Cannon et al., 1998) (<http://www.cns.soton.ac.uk/~jchad/cellArchive/cellArchive.html>). Giorgio Ascoli kindly provided a subset of cells from the PYA study that were corrected in his laboratory for issues like mistaken attachments, inconsistent tags, and zero diameters (Donohue et al., 2002).

The cells of the remaining two studies were kindly provided by the authors; Neil Bannister sent us the reconstructions of the BAN study (Bannister and Larkman, 1995), while Norio Ishizuka provided the reconstructions of the ISH study (Ishizuka et al., 1995).

The digital format of the reconstructed cells was diverse; the MEG and PYA studies were in swc format (Cannon et al., 1998). The rest were in different formats: adhoc (BAN), Miller-Nevin (Jacobs and Nevin, 1991) (CAR), and Eutectics (ISH). While diverse in format, most of the digital reconstructions consisted of three-dimensional (3D) coordinates plus diameter of piecewise cylindrical segments. The sole exception was the BAN study, in which the 3D coordinates were not recorded; the data consisted of the dimensions (length and diameter) plus connectivity only.

We wrote custom software to convert all files to swc format. Once the files were in this format, we examined and edited them using the cvapp Java application available at the Duke/Southampton Archive website. We wrote further software to measure cells in this format and to convert them to a format suitable for input to NEURON (Hines, 1994). In simulations, the membrane properties were set at $R_m = 20 \text{ k}\Omega \cdot \text{cm}^2$, $R_a = 100 \Omega \cdot \text{cm}$, and $C_m = 1$

$\mu\text{F}/\text{cm}^2$. The number of segments per section (nseg) were set to be no greater than one-tenth the length constant at 100 Hz (Hines and Carnevale, 2001).

Table 1 presents a summary of the reconstruction methods used in each of the reviewed studies. Sprague-Dawley rats were used in most studies, while Wistar rats were used in the MEG study and Fisher-344 rats were used in the in vitro series of the PYA study. Young adult rats within the range of 30–60 days old were used in most studies, although the CAR and the in vivo series of the PYA study used rats that ranged from 40 to 360 days old. Male rats were used in the BAN, MEG, and the in vitro series of the PYA study, while the ISH study used female rats. The CAR and in vivo series of the PYA study used rats of both sexes.

The PYA study had two protocols; 10 cells were labeled in vitro, while the rest (24) were labeled in vivo (two rightmost columns). Furthermore, neurons in the MEG study were labeled in vivo, while those of all other studies were labeled in vitro. Cells were labeled intracellularly in all studies except the MEG study.

The reconstructions of the MEG study included separate apical and basal trees and no soma. In correspondence, Dr. Gulyás indicated that the somas were not reconstructed in the study, but he provided long- and short-axis somatic measures that had been carried out in his laboratory. We used these measures to construct an ellipsoidal soma onto which we attached the reconstructed apical and basal subtrees.

Most studies measured the diameter directly using a cursor in the computer monitor. The BAN study estimated diameters from the camera lucida drawings. The MEG study used a hybrid approach, in which dendritic processes were classified into ten classes based on anatomical considerations like stratum and order using light microscopy. A series of samples from each class were measured using camera lucida drawings and under the electron microscope (EM), and average diameter values were obtained for each class. Dendrites were selected that ran parallel with the surface of the section and diameters were measured at evenly spaced intervals along the longitudinal axis of the dendrite.

The microscope's magnification varied from $\times 63$ for the CAR and ISH studies, to $\times 100$ for the MEG and PYA studies. The CAR and PYA studies reported a numerical aperture of 1.25, while the rest did not mention this parameter.

Most studies used the focus of the microscope for the z -axis measurements. The BAN study made no attempt to obtain z -values, but dendritic lengths were corrected for projection errors by using Pythagoras' theorem and a length correction of 1.1 was applied for dendritic "wiggles" orthogonal to the section plane. The MEG study used a software program (Wolf et al., 1995) to estimate z -coordinates from previously traced dendritic segments in adjacent slices (see Gulyás et al., 1999, for further details).

The degree of tissue shrinkage is an important consideration in any morphological reconstruction study. Tissue shrinkage was not addressed in the BAN study. The other studies estimated shrinkage by comparing the size of the tissue before and after processing. The CAR and ISH studies minimized shrinkage by clearing slices in ascending concentrations of glycerol

TABLE 1.

*Methods Used for Reconstructions in Reviewed Studies**

Study	BAN	CAR	ISH	MEG	PYA vitro	PYA vivo
Rat strain	Sprague-Dawley	Sprague-Dawley	Sprague-Dawley	Wistar	Fisher-344	Sprague-Dawley
n	6	7	23	18	10	24
Sex	Male	6 M/1 F	F	M	M	Both
Age (days) ^a	~35–42	42–368	30–57	~65	60	60–240
Weight (g)	100–150	NA	NA	300	NA	200–350
Hemisphere	NA	NA	Left	Both	Both	Right
Hippocampal location	NA	Middle third	Middle third	AP = -3.2 from β	NA	AP = -3.3 from β
Dye	Biocytin	2–3% HRP	2% HRP	BDA (biotinylated dextran amine)	Neurobiotin	Biocytin
When dyed	In vitro	In vitro	In vitro	In vivo	In vitro	In vivo
Process	Slice 400 μm → dye → fix → slice 60 μm → react → image	Slice 400 μm → dye → react → fix → image	Slice 400 μm → dye → react → fix → image	Dye → fix → slice 60 μm → react → image	Slice 500 μm → dye → fix → slice 100 μm → react → image	Dye → fix → slice 70 μm → react → image
Reconstruction method	Camera lucida 10% wiggle correction	Miller–Nevin focus = z-axis ×63 μscope	Eutectics focus = z-axis ×63 μscope	3D-Arbor sftwr from 6–13 sects ×100 μscope	NeuroLucida focus = z-axis ×100 μscope	NeuroLucida focus = z-axis ×100 μscope
Diameter from	Camera lucida	Monitor cursor	Monitor cursor	E.M and camera lucida	Monitor cursor	Monitor cursor
Shrinkage correction	None (unaddressed)	Shrinkage < 5%	Shrinkage < 5%	No shrinkage observed	13% XY/300% Z	33% XY/300% Z
Notes	Did not obtain 3D coords, soma not sampled	Somas had overlapping segments	Somas had overlapping segments	Did not sample soma		

NA, not available.

*Column heading abbreviations correspond to published studies as indicated in the text. In the PYA study, there were two protocols: one for the cells that were dyed in vitro (PYA vitro) and another for those that were dyed in vivo (PYA vivo) corresponding to the two rightmost columns.

^aEntries denoted with ~ used age-weight tables to estimate age from reported weight.

and slices were mounted on slides in 100% glycerol. These studies report that under these conditions slices shrunk by less than 5% linearly. In the MEG study, shrinkage in the light microscope measures along the x – y -axes was found to be minimal, whereas the vibratome thickness setting was used as input to the software for the z -axis distance between adjacent sections, obviating shrinkage considerations on the z -axis. An evaluation of shrinkage of the EM measures was also minimal (0.5%) in all axes. The PYA study exhibited substantial shrinkage, most of all on the z -axis. An analysis of slices prepared with the in vitro protocol indicated that tissue shrunk 10–11% on the x - and y -axes, and 75% in the z -axis primarily due to dehydration. In the in vivo protocol, shrinkage was estimated at 25% on the x - and y -axes and 75% on the z -axis.

Reconstructions used for Table 4 and Figure 2 were rotated along the x – y plane to align the main apical trunk with the y -axis. This process used the first principal component on the x – y plane of all segments to estimate the orientation of the apical trunk. The coordinates along the z -axis were not affected by this operation.

Statistical analysis was carried out using SPSS 11.5 for Windows. Post hoc analyses were performed using the Games–Howell procedure ($\alpha = 0.02$) because sample sizes were unequal, and Levene's test indicated that variances were heterogeneous.

RESULTS

Basic Measurements

Table 2 presents the results we obtained when measuring the length, surface area, volume, number of terminals, and their order for all the reconstructions reported in Bannister and Larkman (1995), Carnevale et al. (1997), Ishizuka et al. (1995), Megias et al. (2001), and Pyapali et al. (1998), which we refer to as BAN, CAR, ISH, MEG, and PYA, respectively hereafter.

The mean values of the length index ranged from a low of 11,479 μm for the MEG study to a high of 16,992 μm for the PYA study. The relative contribution (as percentage of the total) of the apical subtree spanned from a low of 53% (BAN) to a high of 66% (ISH), while the basal compartment contributed the remaining 34% (ISH) to 47% (BAN). The somatic compartment contributed very little length in any of the studies.

In terms of surface area, the means of the reviewed studies varied more than 4-fold from a low of 16,074 μm^2 for the ISH study to a high of 67,102 μm^2 for the CAR study. Nevertheless, the relative allocations to apical, somatic, and basal compartments showed greater consistency, with lows of 60% (BAN), 1% (CAR), and 25% (MEG), and highs of 72% (MEG), 6% (ISH), and 40% (BAN) respectively. The area of the somatic compartment varied

TABLE 2.

Basic Measurements of Reconstructed Cells in Reviewed Studies*

Study n	BAN 6		CAR 7		ISH 23		MEG 18		PYA 34	
	Mean \pm SD	% Tot	Mean \pm SD	% Tot	Mean \pm SD	% Tot	Mean \pm SD	% Tot	Mean \pm SD	% Tot
Length (μm)										
Total	11,980 \pm 989		12,808 \pm 1,541		13,471 \pm 1,086		11,479 \pm 2,270		16,992 \pm 5,788	
Apical	6,408 \pm 776	53	7,943 \pm 1,526	62	8,835 \pm 1,180	66	7,242 \pm 1,655	63	10,548 \pm 4,020	62
Soma	NA ^b	—	40 \pm 9	0	36 \pm 10	0	20 \pm 2	0 ^a	54 \pm 36	0
Basal	5,572 \pm 718	47	4,826 \pm 995	38	4,600 \pm 960	34	4,217 \pm 1,016	37	6,389 \pm 2,553	38
Area (μm^2)										
Total	36,097 \pm 3,590		67,102 \pm 10,953		16,074 \pm 1,787		17,366 \pm 3,157		33,684 \pm 20,392	
Apical	21,823 \pm 2,012	60	42,151 \pm 9,699	63	10,506 \pm 1,869	65	12,516 \pm 2,691	72	21,073 \pm 14,206	63
Soma	NA ^b	—	932 \pm 153	1	1,026 \pm 238	6	529 \pm 49	3 ^a	1,308 \pm 1,241	4
Basal	14,274 \pm 2,208	40	24,019 \pm 3,933	36	4,542 \pm 970	28	4,320 \pm 994	25	11,303 \pm 7,397	34
Volume (μm^3)										
Total	11,083 \pm 1,382		30,384 \pm 6,093		3,828 \pm 993		4,057 \pm 633		10,804 \pm 10,137	
Apical	7,885 \pm 1,149	71	18,696 \pm 5,122	62	1,500 \pm 571	39	2,598 \pm 606	64	5,604 \pm 6,778	52
Soma	NA ^b	—	1,848 \pm 354	6	1,919 \pm 619	50	1,058 \pm 105	26 ^a	2,871 \pm 4,310	27
Basal	3,198 \pm 654	29	9,839 \pm 1,400	32	409 \pm 121	11	401 \pm 92	10	2,329 \pm 2,195	22
Number of terminals										
Total	89.2 \pm 10.8		81.6 \pm 11.4		90.8 \pm 10.7		77.8 \pm 14.4		86.8 \pm 23.0	
Apical	46.2 \pm 12.6	52	51.4 \pm 13.9	63	61.5 \pm 11.0	68	50.4 \pm 12.5	65	53.4 \pm 20.1	62
Basal	43.0 \pm 7.8	48	30.1 \pm 6.5	37	29.3 \pm 6.8	32	27.4 \pm 6.4	35	33.4 \pm 9.8	38
Order of terminals										
Total	8.6 \pm 1.4		9.8 \pm 2.2		10.9 \pm 1.8		11.4 \pm 1.8		9.6 \pm 1.7	
Apical	12.4 \pm 1.9		12.6 \pm 2.6		14.0 \pm 2.7		14.7 \pm 2.3		12.2 \pm 2.5	
Basal	4.3 \pm 0.5		4.6 \pm 0.5		4.7 \pm 0.6		5.4 \pm 0.3		5.4 \pm 1.0	

*Mean \pm SD for the indices that were measured as well as the percentage of the total (% Tot) for the apical, somatic and basal compartments. The order of terminals started from the soma (with a value of 1) and added one for each bifurcation that was encountered after leaving the soma until a terminal was reached. Column heading abbreviations correspond to published studies as indicated in the text. Percentages may not add exactly to 100% due to rounding.

^aSomas were added in the course of our study based on data supplied by the author (see Materials and Methods).

^bSomas were not reconstructed in this study.

almost threefold from a low of 529 (MEG) to a high of 1,308 (PYA) μm^2 . The coefficient of variation (CV = SD/mean) of the area measures had a range of 10–18%, except for the PYA study, for which it was 61%.

The mean volumes varied more than eightfold from a low of 3,828 μm^3 for the ISH study to a high of 30,384 μm^3 for the CAR study. As with the surface area, the somatic compartment volume values were more in agreement from a low of 1,058 (MEG) to a high of 2,871 (PYA) μm^3 . However, the compartmental percentages showed substantial disagreement. Excluding the BAN study that did not reconstruct the soma, the apical compartment volume ranged from a low of 39% for the ISH study to a high of 64% for the MEG study, whereas the soma volume ranged from 6% (CAR) to 50% (ISH), and the basal tree volume from 10% (MEG) to 32% (CAR). The coefficient of variation of the total volume measures had a range of 12–26%, except for the PYA study, for which it was 94%.

The mean total number of terminals showed little variation with a low of 77.8 (MEG) to a high of 90.9 (ISH). The BAN study had almost equal percentage allocations of this index to the apical and

basal subtrees, while the rest had a higher value for the apical (61–68%) than the basal (32–38%) subtrees.

Finally, most studies had similar average values for the order of terminals that ranged from 8.6 (BAN) to 11.4 (MEG). The apical compartments had a higher value than the basal compartments; the former ranged from 12.2 (PYA) to 14.7 (MEG), while the latter ranged from 4.3 (BAN) to 5.4 (PYA).

After a detailed examination of the results presented in Table 2, we identified three issues for further analysis. First, the PYA study exhibited larger variabilities than the other studies, especially in the area and volume indices, as indicated by larger coefficients of variation. Second, the lengths in the PYA study were larger than those of the other studies which appeared to cluster around a common value. Third, the variability across studies in the surface area and volume results was unexpectedly large. We address each issue in turn.

Variability of the PYA Study

Large variabilities typically arise from outliers in the dataset. We therefore used the Grubbs test (Grubbs, 1969) to iteratively iden-

TABLE 3.

Basic Measurements for the PYA-R Dataset*

Study n	PYA-R 30	
	Mean \pm SD	% Tot
Length (μm)		
Total	16,122 \pm 4,475	
Apical	9,999 \pm 3,422	62
Soma	48 \pm 30	0
Basal	6,074 \pm 2,012	38
Area (μm^2)		
Total	28,567 \pm 11,987	
Apical	17,704 \pm 7,862	62
Soma	1,064 \pm 741	4
Basal	9,799 \pm 5,236	34
Volume (μm^3)		
Total	7,957 \pm 5,066	
Apical	4,063 \pm 2,891	51
Soma	2,080 \pm 2,409	26
Basal	1,814 \pm 1,209	23
Number of terminals		
Total	85.5 \pm 23.6	
Apical	52.5 \pm 20.9	61
Basal	33.0 \pm 9.4	39
Order of terminals		
Total	9.6 \pm 1.8	
Apical	12.1 \pm 2.6	
Basal	5.5 \pm 1.0	

*Results for the PYA study when the four outliers (n125, n126, n401, and n422) identified by the statistical outlier test were removed.

tify outliers based on surface area and volume; the measures that showed the most variability in the PYA study. The Grubbs test at $\alpha = 0.05$ detected 4 outliers, namely the cells identified by n125, n126, n401, and n422. The total length, area and volume of the outlier group was $23,520 \pm 10,509 \mu\text{m}$, $72,060 \pm 30,980 \mu\text{m}^2$, and $32,157 \pm 13,889 \mu\text{m}^3$, respectively. We will refer to the PYA dataset after removing these four cells by PYA-R hereafter.

Table 3 shows the results of summarizing the PYA study after removing the four outliers identified in the analysis. The means of all indices were reduced by this operation, most notably the volume and, to a lesser degree, the surface area. The CV was reduced from 61% to 42% for the area index and from 94% to 64% for the volume measure.

Thus, outliers were only partially responsible for the larger variability of the PYA-R study, as the coefficients of variation remained noticeably higher than those of the other studies.

Detailed Analysis of Cell Lengths

Cell length is one of the most important morphological properties used to assess neural function. Mean length in most studies in Table 2 seemed to cluster in the 11,500–13,000- μm range, except for the PYA study, for which this measure was 16,992 μm (16,122

μm for PYA-R). We decided to investigate the source of this disagreement.

The result of a single factor ANOVA between the study groups to test if the total length results were probably drawn from different distributions was positive ($F_{4,83} = 7.97$; $P < 0.0001$). Post hoc analysis ($P < 0.02$) revealed that the PYA dataset was significantly different from all other studies. The test also indicated a significant difference between the MEG and ISH studies. A similar analysis using the PYA-R dataset produced very similar results, the only difference being that the significance of the PYA-R vs. ISH comparison was reduced to $P < 0.028$.

Having found that the total length values for the PYA study diverged significantly from those of the other studies, we decided to look more closely at these reconstructions. Direct examination revealed that most of the cells showed sharp large back-and-forth transitions, or kinks, along the z -axis. Figure 1 illustrates this observation, where the same cell was projected on the x - y plane on the left panel and on the y - z plane for the right panel. Note how the y - z projection exhibits abrupt transitions along the z -axis, making the cell appear highly distorted. These kinks were not as evident on the other axes or in the other studies. This informal examination suggested that an inordinate amount of kinks along the z -axis of the PYA study might be responsible for their longer lengths. We therefore performed an analysis of lengths along each dimension.

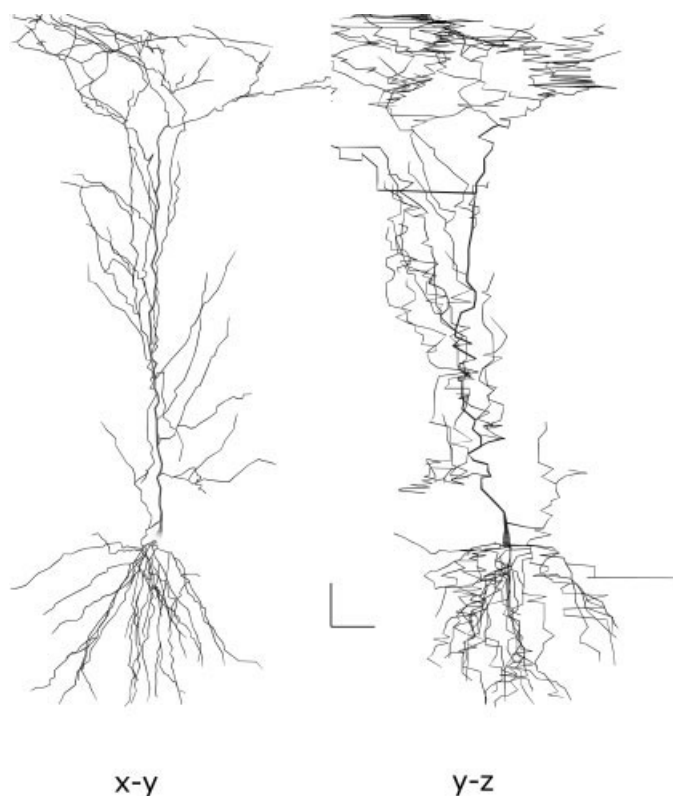


FIGURE 1. Projection of cell n400 onto the x - y and y - z planes. Cell n400 when viewed on the x - y plane (left) and the y - z plane (right). Degree of shading is proportional to diameter. Scale bar = 50 μm .

TABLE 4.

Results From Coordinate Axes Analysis*

Study	CAR	ISH	MEG	PYA-R
	Mean \pm SD	Mean \pm SD	Mean \pm SD	Mean \pm SD
Length (μm)				
x	5,311 \pm 703	5,750 \pm 606	4,950 \pm 1,041	5,280 \pm 1,617
y	9,255 \pm 1,409	9,814 \pm 1,003	6,949 \pm 1,446	7,758 \pm 2,409
z	3,791 \pm 347	3,853 \pm 756	5,138 \pm 1,071	8,794 \pm 3,372
Span (μm)				
x	412 \pm 61	429 \pm 71	468 \pm 128	418 \pm 116
y	903 \pm 83	928 \pm 87	745 \pm 68	860 \pm 126
z	233 \pm 46	260 \pm 46	458 \pm 83	400 \pm 264
Kink				
k_x	13.1 \pm 2.2	13.7 \pm 2.4	11.0 \pm 2.6	13.0 \pm 4.0
k_y	10.3 \pm 1.9	10.6 \pm 1.2	9.3 \pm 1.5	9.0 \pm 2.1
k_z	16.8 \pm 3.1	15.0 \pm 2.4	11.3 \pm 2.0	28.0 \pm 14.8

*Results from the dimensional analysis for each of the studies that were reviewed. The span along each dimension corresponds to the maximum minus the minimum value that was obtained in that coordinate, i.e., $span_i = max_i - min_i$. The kink index along each dimension was computed as the length along that dimension over the span on the same dimension, i.e., $k_i = length_i / span_i$. Note that before measuring, reconstructions were rotated along the x - y plane to align the main apical trunk to the y -axis. The BAN study was not included because it did not record three-dimensional coordinates.

Coordinate Axis Analysis

Table 4 summarizes the results we obtained when we measured cells along each coordinate axis. We measured the total length, the span, and a “kink” index. For each cell the kink k_i index was calculated by dividing the cell’s length along the i -axis by the cell’s span along the same axis.

A two-factor analysis of variance (ANOVA) found significant effects for study and dimension on the length ($F_{11,200} = 27.9$; $P < 0.0001$), span ($F_{11,200} = 119$; $P < 0.0001$) and kink indices ($F_{11,200} = 25$; $P < 0.0001$).

Post hoc analysis ($P < 0.02$) comparing the length on each dimension across studies revealed no differences along the x -axis, but found two separate groups (CAR + ISH vs. MEG + PYA-R) along the y -axis, and three separate groups along the z -axis (CAR + ISH vs. MEG vs. PYA-R). The same statistic, when comparing axial length measures within each study, found that all combinations of the x -, y -, and z -axis comparisons were significantly different from each other in all studies except for the x vs. z comparison in the MEG study and the y vs. z comparison in the PYA-R dataset.

The post hoc comparison of studies along each dimension of the span index showed no significant differences along the x -axis, while there were two groups (CAR + ISH + PYA-R vs. MEG) along the y -axis and, similarly, two groups (CAR + ISH vs. MEG + PYA-R) along the z -axis. The same statistic, when comparing axial span measures within each study, revealed two groups (CAR + ISH vs. MEG + PYA-R). In the first group, all combinations of the x -, y -, and z -axis comparisons were significantly different from each other, while in the second group only the x vs y , and y vs. z comparisons differed statistically.

Post hoc analysis of studies along each dimension of the kink index showed that only the ISH and MEG studies differed statistically along the x -axis, while there were no differences along the y -axis. However, along the z -axis, all comparisons were significant, except for the CAR vs. ISH and CAR vs. PYA-R pairings. The same statistic, when comparing axial kink measures within each study, revealed three groups. In the first group (CAR + MEG) only the y vs. z differences were significant. The second group (ISH) was similar to the first, except that the y vs. z pairings were also significant. In the third group (PYA-R), all possible pairings differed statistically.

Span and Kink Anomalies in the PYA-R Dataset

In summarizing the data of the PYA-R dataset, we noted that the mean values for the z -axis span and kink indices did not agree with their medians, suggesting the possibility of a multi-modal distribution. Figure 2 reveals what we found on closer inspection. It shows a scatterplot of the span index on the abscissa vs. the kink index on the ordinate, with a panel for each of the coordinate axes. While the panels for the x and y dimensions show a compact cloud, the z -axis plot reveals three groups of points. The most crowded one is composed of points from all studies, whereas the other two comprise only PYA-R data. The smaller of these had three points on the far end of the $span_z$ index, while the other had 8 points and was located on the far end of the k_z index. We will refer to the PYA-R dataset with these two groups of cells removed as PYA-R2 hereafter.

The three-point group (cells n406, n410, and n416) had a $span_z$ average of $1,055 \pm 123 \mu\text{m}$, more than twice, and 2.5 SD away

from, the study mean for this index, and larger than the study mean for the $span_y$ index. On visual examination these cells appeared normal when viewed on the x - y plane, but were highly extended and distorted when viewed on the y - z plane.

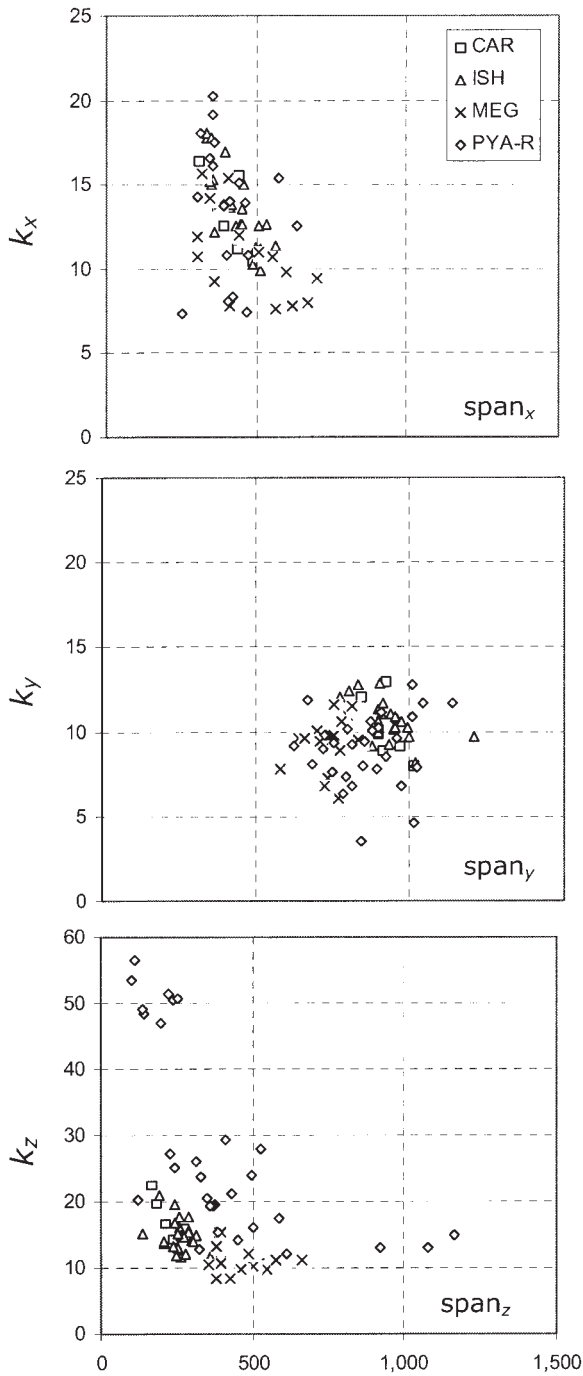


FIGURE 2. Scatterplot of $span$ vs $kink$ on each coordinate axis. Scatterplots of the $span$ vs $kink$ indices for the x -axis (top), the y -axis (middle) and the z -axis (bottom), for each of the reviewed studies. The BAN study was not included because it did not include 3D coordinates. Study abbreviations correspond to published studies as indicated in the text.

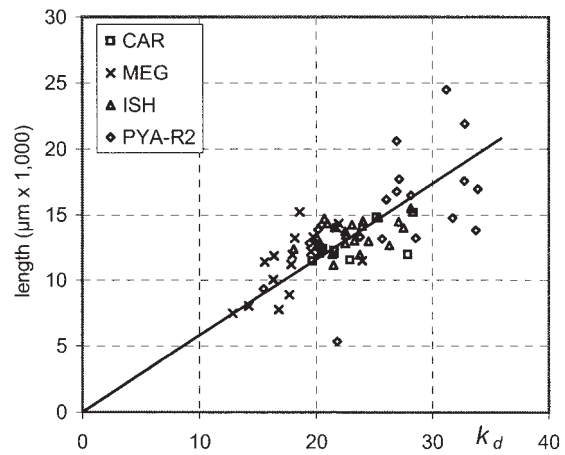


FIGURE 3. Scatterplot of k_d vs $length$. Scatterplot of k_d vs total length for each of the reviewed studies. The line corresponds to the best fit of the data to the equation $l_t = c_k \cdot k_d$, where $k_d = \sqrt{k_x^2 + k_y^2 + k_z^2}$ is the length of the box's diagonal, l_t is the cell's total length, and c_k is a constant. The best fit (least squares) was obtained with $c_k = 580 \mu m$. The BAN study was not included because it did not include 3D coordinates.

The eight point group (cells n120, n121, n127, n128, n129, n130, n412, and n413) had an average $span_z$ index ($176 \pm 60 \mu m$) of less than one-half the PYA-R study mean and the average k_z was 50.9 ± 3.0 , or 80% larger and 1.5 SD above the study mean for this index. On visual examination, these cells appeared normal when viewed on the x - y plane, but appeared grossly flattened when viewed on the y - z plane.

Having found that the k_z index was abnormally large in the PYA-R dataset, we considered whether the magnitude of this effect was sufficient to account for the distinctively larger total length values of the PYA study. In order to estimate a correction factor, we considered that it would be reasonable to expect a direct relationship between the total length of a cell and the length of the diagonal of a box with sides sized at k_x , k_y , and k_z ; specifically $l_t \sim c_k \cdot k_d$ where $k_d = \sqrt{k_x^2 + k_y^2 + k_z^2}$ is the length of the box's diagonal, l_t is the cell's total length and c_k is a constant. With an estimate of the value of c_k we could substitute PYA's anomalous k_z value with a more typical one to obtain a revised value of total length.

Figure 3 shows a scatterplot of k_d versus total length for the cells from the CAR, ISH, MEG, and PYA-R2 datasets, along with a plot of the results of a best fit to the above equation. The equation's fit was adequate with an $R^2 = 0.97$ (although this score is not directly comparable to that obtained from fits that include an intercept), and the value of c_k was estimated at $580 \mu m$. Using this c_k value, the revised estimate of the total length for the PYA-R study was $12,996 \mu m$, which was obtained by using its own k_x and k_y mean values, but substituting its k_z value with that of the average of the CAR and ISH studies. The revised total length value was within the range of values for this index of the other studies, indicating that the magnitude of the k_z index abnormality was sufficient to explain the larger total length values of the PYA study.

Summarizing, we have found that the total cell lengths in the PYA study were larger than those of the other studies, that the

excess was likely due to the presence of substantial kinks on the z -axis, and finally, that the surplus z kinks were sufficient to account for the excess lengths.

Detailed Analysis of Cell Diameters

The third issue that warranted further investigation was the large variability across studies that we observed in Table 2 for the surface area and volume indices. The results of a single-factor ANOVA between the study groups to test whether the results were drawn from different distributions was positive for area ($F_{4,83} = 24.6$; $P < 0.0001$) and volume ($F_{4,83} = 24.9$; $P < 0.0001$). All but two comparisons (BAN vs PYA and ISH vs MEG) were significant in a post hoc analysis ($P < 0.02$). Similar results were obtained using the PYA-R dataset.

Given that the two variables involved in the calculation of area and volume are the length and diameter of each segment, and that length variability was much smaller than the variability we encountered for areas and volumes, we concluded that diameter variability should be the source of the excess area and volume variation.

To understand further the nature of diameter variability we quantified the contribution of segments with given diameters to the length, surface area, and volume of each cell. For each cell, we placed all segments into bins based on their diameter and calculated the contribution of each bin to its nonsomatic length, surface area, and volume. We excluded somatic segments from this analysis to concentrate on dendritic processes and avoid possible contamination by the typically thick somatic compartments.

Figure 4 presents the average results we obtained with the above procedure when grouped by study, ordered from top to bottom by their surface area rank in Table 2. Note that the y scale is the same for all panels, except for the top one.

We found that for each study, there were a small number of prominent bin diameters that when combined accounted for a significant portion of the length, area and volume indices. This was most extreme for the ISH study where a single bin centered on 0.3 μm accounted for 88% of the length, 75% of the area, and 49% of the volume. A similarly extreme case was the CAR study, in which two individual bins centered at 1.4 and 1.8 μm accounted, when combined, for 91%, 88%, and 82% of length, surface area, and volume, respectively. In contrast, the BAN study had a contiguous group of bins centered at 0.7 μm whose contribution tapered sharply for smaller diameters just below 0.5 μm , but more slowly for wider segments with noticeable contributions to more than 1.9 μm . The PYA-R dataset presented a similar pattern with the main group centered at 0.5 μm , but also showed an isolated bin centered at 0.2 μm that contributed an average of 32%, 16%, and 5% of length, area, and volume, respectively. The MEG study showed several isolated bins with the major one centered at 0.5 μm and the rest at 0.3, 1.2, and 2.2 μm . This was not unexpected, given that this study assigned a predefined set of diameters to each segment based on anatomical considerations (see Materials and Methods).

The bin diameter of major peaks in Figure 4, when considering the panels from top to bottom, shifted toward larger diameters, consistent with their surface area rank order in Table 2. These

peaks could be roughly positioned at 0.3, 0.5, 0.6, 0.7, and 1.8 μm for the ISH, MEG, PYA-R, BAN, and CAR studies, respectively. The concordance of the peak-diameter to surface-area (volume) ordering indicates that the large variation in surface area (volume) across studies in Table 2 is attributable to broad dissimilarities in diameter measurements between studies.

To evaluate the degree of consistency by which diameters were designated within each study, we calculated the coefficient of variation (CV) for the bin contributions shown in Figure 4. Large values of this index indicate a large degree of variability of the underlying measure.

Figure 5 presents the results we obtained for the CV of the contributions of each bin to surface area grouped by study. Note that only bins whose contribution was larger than 5% of total area were included, as bins with very small contributions tend to have spuriously large CVs.

Most studies showed one to three regions with CVs of at most 60%, with the exception of the PYA-R dataset, which showed three regions with CVs that peaked at 111%, 122%, and 228% centered at 0.2, 0.6, and 0.8 μm , respectively. The comparatively large CVs of the PYA-R dataset indicate that the large variability in surface areas shown in Table 2 for this study is due to large variations in the designation of segment diameters.

Summarizing, we have found that segments with a small number of diameters accounted for a significant portion of lengths, areas, and volumes of reconstructed cells. Most studies appeared to have a preset range of values for the diameters they reported, and the differences in ranges translated into large variabilities in cell measures across studies, and perhaps most notably, within the PYA-R study.

Passive Electrotonic Properties

Following our detailed morphological analysis of the CA1 pyramidal cell reconstructions described above, we investigated the degree to which the features we observed were reflected in simulations of their electrophysiological properties.

Figure 6 illustrates the results we obtained when using the simulations to estimate the input resistance (R_N) of each cell, and plotting these values against their surface areas. Passive membrane properties were chosen to be consistent with experimental results for hippocampal pyramidal cells (Spruston and Johnston, 1992). To reduce the complexity of this initial analysis, we did not compensate for dendritic spines and did not include active channels.

The R_N values varied nearly 10-fold from a minimum of 30.8 $M\Omega$ for cell 5038801 of the CAR study to a maximum of 292.2 $M\Omega$ for cell n414 of the PYA-R dataset. The overall shape of the scatterplot was immediately suggestive of a power relationship between these two variables. The significance of this observation was confirmed statistically ($F_{1,82} = 718$; $P < 0.00005$ and an $R^2 = 0.90$) for the functional form $R_N = b_1 A_N^{b_2}$, where A_N was the area in μm^2 and constants $b_1 = 1,912,016$ and $b_2 = -0.96$. As expected, this shows that R_N and A_N are inversely correlated. Two points laid far off the fitted curve; one was at $R_N = 248 M\Omega$; $A_N = 28,300 \mu\text{m}^2$ for cell n416, while the other was at $R_N = 186 M\Omega$;

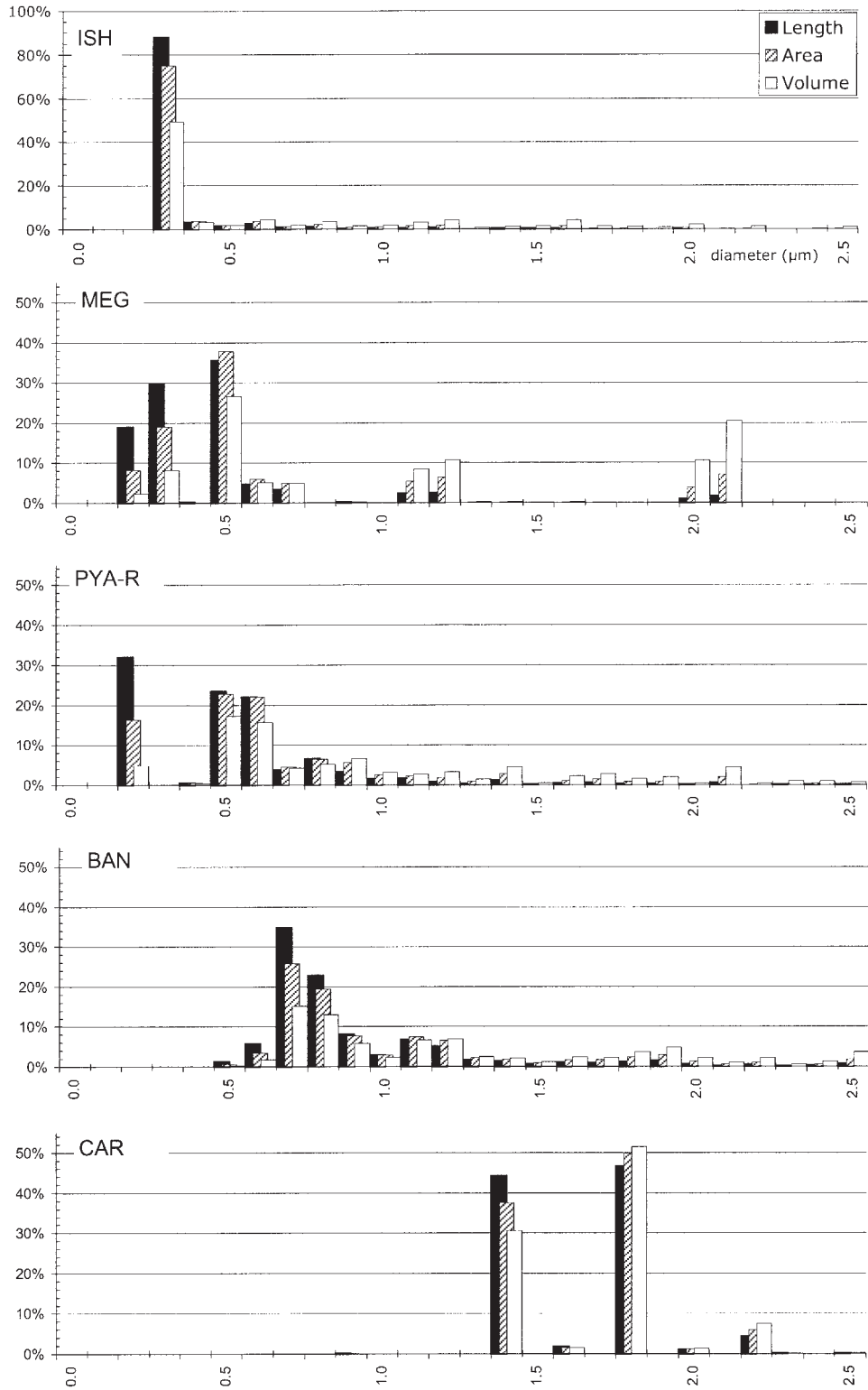


FIGURE 4. Detailed analysis of diameters per length, surface area, and volume. All segments were placed into bins (of 0.1-μm increments) based on their diameter. Their contribution to length, surface area, and volume was calculated. Mean value of each bin for all cells in each study, where the studies were sorted from top to bottom according to their rank order for surface area in Table 2.

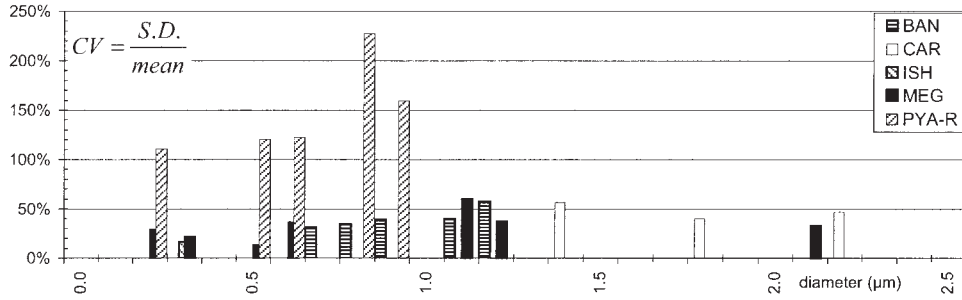


FIGURE 5. Assessment of variability in diameter measurements. Coefficient of variation ($CV = SD/mean$) of the contributions to surface area of the bins in Fig. 4. Bins with less than 5% mean contribution were excluded, as small contributions tend to have spuriously large CVs.

$A_N = 22,544 \mu\text{m}^2$ for cell n412. Both cells were identified as outliers in Figure 2.

Some of the cells appeared to cluster at similar R_N values for given studies. Table 5 shows the results we obtained when we summarized the R_N values by study group. The mean values varied more than 4-fold from a low of $38 M\Omega$ for the CAR study to a high of $172.1 M\Omega$ for the ISH data, and the means of each study varied inversely to their diversity in surface areas.

Table 5 also summarizes our results for estimating the electrotonic length (L_N) of each cell. We used an approximation by Rall (1977):

$$R_m \approx \frac{R_N A_N \tanh L_N}{L_N}$$

where L_N is the electrotonic length of the cylinder that is most nearly equivalent to the soma plus dendrites, R_m is the membrane resistivity, and A_N is the cell's surface area, and solved for L_N using the area and input resistance values we had obtained for each cell. The mean electrotonic lengths so obtained were rather similar and

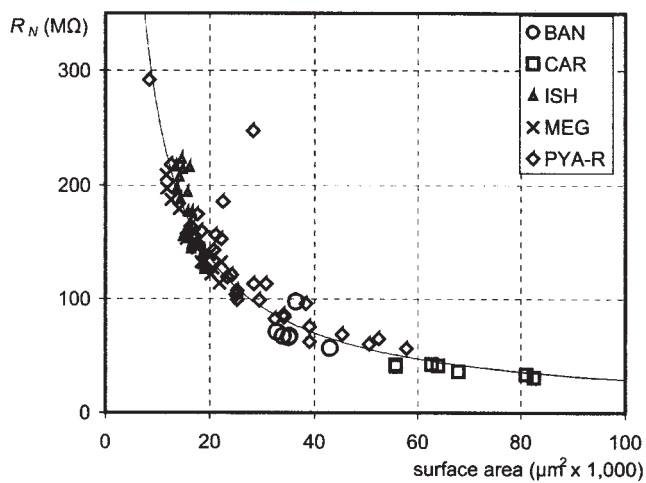


FIGURE 6. Scatterplot of surface area vs input resistance. Input resistance (R_N) was measured in simulations with passive membrane conditions. Membrane properties were set at $R_m = 20 \text{ k}\Omega \cdot \text{cm}^2$, $R_a = 100 \Omega \cdot \text{cm}$ and $C_m = 1 \mu\text{F}/\text{cm}^2$. The fit corresponds to the best fit (least-squares) to the equation $R_N = b_1 A_N^{b_2}$, where A_N is the surface area and $b_1 = 1,912,305$ and $b_2 = -0.96$ are constants.

clustered at 1.27 for the BAN, CAR, and MEG studies, while the ISH and PYA-R were somewhat larger at 1.36 and 1.56, respectively.

Simulations of EPSPs

To illustrate the degree to which the variability in morphological reconstructions was reflected in electrophysiological properties, we recorded the somatic voltage after synaptic stimulation in two cells, and compared the results. We selected two cells from the PYA-R dataset that have been used in published reports, namely n123 (Poirazi et al., 2003) and n400 (Migliore et al., 1999; Migliore, 2003; Poolos et al., 2002; Watanabe et al., 2002). The synaptic input was identical for both cells and was generated by simulating NMDA and AMPA channel openings after release of a single vesicle of glutamate in the synaptic cleft (Holmes, 1995). The synaptic input location of the control cell (n400) was selected to lie on the apical shaft in the middle of stratum radiatum. The synaptic input location of the comparison cell (n123) was also on the apical shaft, and was placed first, to match the laminar distance, and second, to match the path length to the soma. As shown in Table 6, there were 2–4-fold differences in the peak amplitude, time to peak, and half-width of the somatic EPSP when laminar distance was matched. Differences were smaller, but still substantial, when path length to the soma was matched.

DISCUSSION

We have analyzed morphological reconstructions of pyramidal cells from hippocampal field CA1 of five published studies from the perspective of their value in advancing our understanding of neural function. While the availability of these reconstructions has definitely contributed to our understanding of these cells in qualitative terms, their value for more rigorous quantitative studies depends critically on their accuracy in indices that are known to determine their electrophysiology.

Variability and Diversity

In our analysis, we found substantial variability among reconstructions in properties that matter for neural function, most no-

TABLE 5.

Results for Simulated Input Resistance and Estimated Electrotonic Length*

Study	BAN	CAR	ISH	MEG	PYA-R
	Mean \pm SD	Mean \pm SD	Mean \pm SD	Mean \pm SD	Mean \pm SD
R_N (M Ω)	71.1 \pm 13.9	38.0 \pm 4.6	172.1 \pm 31.1	150.0 \pm 26.5	127.6 \pm 57.1
L_N	1.28 \pm 0.25	1.26 \pm 0.08	1.36 \pm 0.16	1.27 \pm 0.07	1.56 \pm 0.41

*Results of computing the input resistance R_N in simulations, using the reconstructions from the reviewed studies, as well as estimates of the electrotonic length (L_N) of the cylinder that is most nearly equivalent to the cell's soma plus dendrites. Passive membrane parameters were set at $R_m = 20 \text{ k}\Omega \cdot \text{cm}^2$, $R_i = 100 \text{ }\Omega \cdot \text{cm}$ and $C_m = 1 \text{ }\mu\text{F}/\text{cm}^2$.

tably in the surface area and volume indices, while cell lengths were more in agreement. Estimates of the proportion of variability due to biological diversity vs. methodological variance were difficult to ascertain, given that the reviewed studies varied in many aspects of their methodologies.

There was agreement in the mean number of terminals and their order. Similarly, mean cell lengths were comparable, but for one discordant study (PYA). For this study, an exaggerated kink index was found to be significant and also sufficient to account for the longer lengths. The source of the excess kinks is likely to be methodological, perhaps the consequence of nonuniform shrinkage (see below), as this was the lone study that exhibited kinks to such a large degree.

In contrast, cell surfaces and volumes had no central tendency, diverging sharply across studies. ANOVA indicated that, in terms of surface area and volume, most study pairings (8 of 10) were significantly different from each other. Similarity in lengths and disparity in areas and volumes led to the unequivocal conclusion that diameter disagreement was the source of the observed area and volume disparities, as was confirmed in our detailed analysis of diameters. There is no question that some of these differences reflect the intrinsic variability of CA1 pyramidal cells. The sampled cells came from three different rat strains and differed in sex, age,

and hemisphere. It is also important to note that several studies had considerable overlap among these descriptors, suggesting that the variability in the volume and area indices had an important methodological component. In particular, it would appear that some laboratories had biases toward selecting diameters within a predetermined range of values.

Implications for Computational Neuroscience

From the point of view of computational studies, the issue of morphological cell diversity has received little attention. Most computer simulations restrict their attention to a single cell. Attempts to incorporate the morphological diversity of reconstructions are few. Two studies from the Giorgio Ascoli laboratory have attempted this. The first compared groups of intact versus lesioned CA1 cells as a model of Alzheimer's disease (Nasuto et al., 2001), while the other attempted to deduce electrophysiological behavior from dendritic morphology in CA3 cells (Krichmar et al., 2002).

Computer simulations can only benefit from incorporating a diversity of morphological reconstructions into their studies. Computer speeds have increased sufficiently to make it practical to run simulations using more than one cell, which must lead to more robust results. In fact, our results suggest that it may be essential for modeling studies to use several reconstructions to address particular questions.

During the course of our analysis, we identified a number of outlier cells that had measures that were far removed from those of other cells in the study. Although these might be considered examples of biological variability we feel that they should be regarded as unusual and should only be used as part of a larger study including many cells.

Total Cell Length

We found agreement in the total cell lengths among four studies (mean total lengths 11,479–13,417 μm), while the fifth (PYA) had significantly larger values. The larger values could be attributed to unusually large values of the kink index along the z -axis (k_z) of this study, indicative of the sharp back-and-forth transitions that were visually observed along this axis.

The origin of the unusually large z -axis kink measures in the PYA study was not evident, though the fact that this study was the

TABLE 6.

Comparison of Simulated Somatic Voltage in Two Reconstructed Cells*

Cell	Synapse location		Somatic voltage measures		
	d_l (μm)	d_p (μm)	v_{pk} (μV)	t_{pk} (ms)	$w_{1/2}$ (ms)
n400	293	487	92.1	6.2	22.8
n123	253	674	25.6	15.6	43.4
n123	172	478	43.8	8.8	30.5

*Measures of the simulated voltage trace recorded at the soma after stimulation of a single synapse. d_l , laminar distance from soma (distance along apical trunk axis); d_p , path length distance from soma; v_{pk} , peak voltage; t_{pk} , time to peak; $w_{1/2}$, half-width. Passive membrane parameters were set as in Table 5.

only one to report a substantial amount of shrinkage along this axis may be significant. Tissue was reported to have shrunk to 25% of its original size along the z -axis, and therefore the cells we examined had been corrected for shrinkage by a factor of 4 on this axis. However, the k_z index is not affected by corrections of this sort because the correction factor cancels out as it appears in both the numerator and denominator. This finding suggests that the anomalous values were present before shrinkage corrections were applied. It is unknown whether tissue shrinkage under these conditions is homogeneous at the microscopic level. Shrinkage at the edge of a slice may differ from that on the inside. Shrinkage may vary among intracellular and extracellular spaces, cell surfaces, and organelles. Dendritic processes could have crinkled as the slice shrank by dehydration. Further deformation may have been introduced in the *in vitro* series, as slices may spread in the x - y dimensions and collapse in the z -axis, while in the recording chamber. If so, a linear correction of coordinates as applied in the PYA study, based on the macroscopic degree of shrinkage, would be inappropriate and would have amplified the pattern of crinkled processes. Operator visual fatigue errors, where the operator fails to maintain precise focus and refocuses only when faced with a clearly out-of-focus dendrite, could have compounded the problem. See Jaeger (2001) for a discussion of these and other issues.

Coordinate Axis Anomalies

In addition to the PYA study anomalies, and contrary to expectations, the coordinate axis analysis demonstrated significant differences in some studies between the x - and z -axis measurements. Specifically, in the CAR and ISH studies, the length and span along the x -axis were significantly larger than along the z -axis, i.e., $length_x > length_z$ and $span_x > span_z$.

The above data suggest the possibility that the dendritic arbor along the plane perpendicular to the apical trunk may be asymmetric in the x - vs. z -axis. The slices from the ISH, and presumably the CAR, studies were cut perpendicular to the long axis of the hippocampus. Thus, the putative asymmetry would indicate that the dendritic arbor along the short axis would be wider and more extensive than along the long axis. The absence of reports for observations of this sort suggests that the source for the above x - z discrepancies may be an artifact.

The CAR and ISH studies used step motors to measure the x and y coordinates, while the z -axis was measured by means of the point of focus in the microscope's objective. The systematic nature of the result makes it possible that a failure in adequate calibration may have been at the root of this discrepancy, as the microscope stage and optics require careful calibration (Jaeger, 2001). In contrast, it is possible that the tissue may have been compressed when the slice was pressed down for sampling on the microscope stage, accounting for the smaller span and length along the z -axis. In contrast, the MEG study used a software program to interpolate the z -values from dendritic x, y traces obtained from adjacent slices (Wolf et al., 1995) leading to results that were fairly symmetric in the x - z dimensions.

The MEG study had substantially smaller length and span values along the y -axis than all other studies. The source of this dis-

crepancy is not clear, although one possibility is that this study used a strain of rat different from all other studies.

Surface Area and Volume

There was substantial variability in the cell's surface area and volume measures across studies. The surface area means varied more than fourfold and the volume means more than 8-fold. Moreover, the PYA study exhibited substantially greater variability in these two indices than the other four studies.

Undue variability in dendritic diameter measurements was identified as the likely source of the diversity of area and volume measures. Dendritic diameters were fairly consistent within the same study for all studies, except for the PYA study, where diameter assignments varied substantially across cells. Curiously, the number of unique diameter values reported in each study was small. Typically, only two or three diameter values accounted for the vast majority of process diameters.

Measuring the diameter of dendritic processes during the reconstruction of CA1 pyramidal cells is a difficult enterprise, given that their size lies so close to the theoretical limit of resolution for the light microscope ($\sim 0.3 \mu\text{m}$). For example, the PYA and MEG studies had segments with diameters of $< 0.3 \mu\text{m}$, and in the ISH study, where it was reported that they believed to have overestimated diameter measurements, most segments measured $0.3 \mu\text{m}$ in diameter. Conversely, diameters in the other studies were much larger. While two-photon confocal microscopy may improve the resolution for z -axis measurements in NeuroLucida-like systems, there appears to be no alternative to improve the resolution on the x - y plane, and thus of diameter measurements, within light microscopy.

A possible solution to this *impasse* may lie in adopting a hybrid approach combining electron and light microscopy, as was done in the MEG study. In this study dendritic processes were classified into 10 classes based on anatomical considerations such as stratum and order, using light microscopy. A series of samples from each class were measured under the EM and typical diameter values were obtained for each class. Finally, segments of each class in the reconstructed cell were assigned the typical EM measured diameters.

While the hybrid approach abandons the ideal of measuring each cell process individually, it may offer a viable alternative to a pure light microscopy approach. However, while the range of diameter measures is well within the resolution of the EM, the distribution of diameters from the MEG study situates this study near the extreme of narrow diameters when compared to the other studies. Additional reconstructions using the hybrid approach may improve confidence in the diameter estimates that were obtained in the MEG study.

Passive Electrotonic Properties

Simulated input resistance values (R_N) varied substantially reflecting the disparity in surface areas and volumes. This highlights the major role these indices have on electrophysiological behavior. Estimates of the electrotonic length L_N were rather similar across at least four of the five studies, and indicated a rather compact value

for this index. The similarity of the estimated electrotonic lengths in spite of the large variability in surface areas was somewhat surprising. The electrotonic length of a cell is a rough measure of the degree of attenuation suffered by applied currents. It relates to the length of the cylinder that most closely approximates the whole neuron, collapsing the soma and dendritic arbor into a single cylinder. While the surface area is an important influence for this index, the overall shape of the cell, as determined by the number and degrees of bifurcation, is also important. Values for these parameters were similar among the reconstructed cells we analyzed. This may account for the similarity in estimated electrotonic lengths.

We should point out that reconstructions with similar L_N values can vary greatly in realistic functional behavior, as the electrotonic length of a cell is a very broad measure. The two cells used to illustrate the sensitivity of EPSP shape measures to morphological variations had similar L_N values; 1.84 for n400 and 1.71 for n123. Nevertheless, their somatic response to synaptic stimulation differed substantially.

Suggestions for Improving the Quality and Usefulness of Reconstructions

Morphological reconstructions of pyramidal CA1 cells are likely to grow in importance in assessing neural function as progress in elucidating biophysical properties makes it possible to create more detailed simulations, and computational power continues to grow.

While the collection of morphological reconstructions that we have analyzed has been extremely useful to the computational neuroscience community and it cannot be overstated how thankful and appreciative modelers are that anatomists have provided access to their data, there are some issues that we believe should be addressed in future reconstruction studies. We should point out that our area of expertise lies within computational neuroscience so our suggestions mostly reflect issues that concern the use of reconstructions for simulations.

We found that the low reliability of dendritic segment diameter measurements is the most likely methodological source for the wide discrepancies in surface area and volume measures we encountered. For example, Brenda Claiborne clearly warns of this problem in her website where she indicates that the diameters in her reconstructions are overestimates and should be considered inaccurate. This is a difficult problem, as discussed previously, because these diameters lie so close to the limit of resolution of the light microscope. A hybrid approach combining electron and light microscopy measurements, as was used in the MEG study, appears promising in improving reliability, although it sacrifices the ideal of measuring each process individually. Additional studies using this approach should help clarify its validity.

The soma of most cells in the reconstructions we reviewed appeared to be poorly reconstructed, if reconstructed at all. In many cases, multiple cylinders overlapped in space, and apical and basal segments were attached haphazardly with little regard to accuracy in terms of the soma's volume or surface area. The soma is an important electrotonic component of the cell as we found that, in our measurements, its contribution to total volume was 6–50%.

Greater care when sampling the soma would enhance the accuracy of future simulations that use reconstructed CA1 pyramidal cells.

There was no consistent frame of reference for the 3D coordinate values in most of the reconstructions we analyzed. For example, we found no consistency in the orientation of the main apical trunk, or in any other anatomical feature. In our analysis, we found it convenient to rotate cells to obtain a local frame of reference where the y -axis was oriented along the main apical trunk and the origin at the soma's center of mass. The local frame can be related to a global frame (e.g., the location of the cell within the frame of reference of the hippocampal formation) by recording its 3D position and orientation in the parent frame. In any event, the development and use of a hierarchy of canonical frames of reference would enhance the utility of future reconstructions.

The anatomical context of most reconstructed cells has been lost. For most reconstructions, it is only possible to estimate grossly the anatomical layer boundaries, and their global location within the hippocampus, is unknown. The modeling community would greatly benefit if it were possible to integrate or preserve anatomical information into future reconstructions.

Finally, advances in electrophysiological techniques are making it possible to distinguish biophysical properties from diverse regions of the dendritic arbor. We can anticipate that, with further studies, the regional differences will only accumulate so that the distinction between an apical trunk, apical oblique, or apical distal dendritic segment will become increasingly important in assessing neural function. Yet the dendritic segments of most reconstructions are poorly labeled, where at most there is a distinction between apical and basilar trees. The usefulness in simulations of future reconstructions would be greatly enhanced if more attention could be placed into labeling dendritic segments in an anatomically consistent way.

Acknowledgments

The authors thank Ellengene Peterson for her careful reading and helpful comments on previous versions of this manuscript. We also want to thank the authors of the reviewed studies for having made their reconstructions easily available.

REFERENCES

- Ambros-Ingerson J, Holmes WR. 2003. Suitability of CA1 morphological reconstructions for computer simulations. Abstract viewer itinerary planner Program: 476.18. CD-ROM. Washington, DC: Society for Neuroscience, 2003.
- Bannister NJ, Larkman AU. 1995. Dendritic morphology of CA1 pyramidal neurons from the rat hippocampus. I. Branching patterns. *J Comp Neurol* 360:150–160.
- Cannon RC, Turner DA, Pyapali GK, Wheal HV. 1998. An on-line archive of reconstructed hippocampal neurons. *J Neurosci Methods* 84:49–54.
- Carnevale NT, Tsai KY, Claiborne BJ, Brown TH. 1997. Comparative electrotonic analysis of three classes of rat hippocampal neurons. *J Neurophysiol* 78:703–720.

- Desjardins AE, Li YX, Reinker S, Miura RM, Neuman RS. 2003. The influences of I_h on temporal summation in hippocampal CA1 pyramidal neurons: a modeling study. *J Comput Neurosci* 15:131–142.
- Donohue D, Scorcioni R, Ascoli GA. 2002. Generation and description of neuronal morphology using L-Neuron: a case study In: Ascoli GA, editor. *Computational neuroanatomy: principles and methods*. Totowa, NJ: Humana Press. p 49–70.
- Grubbs F. 1969. Procedures for detecting outlying observations in samples. *Technometrics* 11:1–21.
- Gulyás AI, Megias M, Emri Z, Freund TF. 1999. Total number and ratio of excitatory and inhibitory synapses converging onto single interneurons of different types in the CA1 area of the rat hippocampus. *J Neurosci* 19:10082–10097.
- Hines M. 1994. The NEURON simulation program In: Skrzypek J, editor. *Neural network simulation environments*, Norwell, MA: Kluwer. p 147–163.
- Hines M, Carnevale NT. 2001. NEURON: a tool for neuroscientists. *Neuroscientist* 7:123–135.
- Holmes WR. 1995. Modeling the effect of glutamate diffusion and uptake on NMDA and non-NMDA receptor saturation. *Biophys J* 69:1734–1747.
- Ishizuka N, Cowan WM, Amaral DG. 1995. A quantitative analysis of the dendritic organization of pyramidal cells in the rat hippocampus. *J Comp Neurol* 362:17–45.
- Jacobs GA, Nevin R. 1991. Anatomical relationships between sensory afferent arborizations in the cricket cercal system. *Anat Rec* 231:563–572.
- Jaeger D. 2001. Accurate reconstruction of neuronal morphology In: Schutter ED, editor. *Computational neuroscience: realistic modeling for experimentalists*. Boca Raton, FL: CRC Press, p 159–178.
- Jaffe DB, Carnevale NT. 1999. Passive normalization of synaptic integration influenced by dendritic architecture. *J Neurophysiol* 82:3268–3285.
- Kager H, Wadman WJ, Somjen GG. 2002. Conditions for the triggering of spreading depression studied with computer simulations. *J Neurophysiol* 88:2700–2712.
- Krichmar JL, Nasuto SJ, Scorcioni R, Washington SD, Ascoli GA. 2002. Effects of dendritic morphology on CA3 pyramidal cell electrophysiology: a simulation study. *Brain Res* 941:11–28.
- Magee JC, Cook EP. 2000. Somatic EPSP amplitude is independent of synapse location in hippocampal pyramidal neurons. *Nat Neurosci* 3:895–903.
- Mainen ZF, Carnevale NT, Zador AM, Claiborne BJ, Brown TH. 1996. Electrotonic architecture of hippocampal CA1 pyramidal neurons based on three-dimensional reconstructions. *J Neurophysiol* 76:1904–1923.
- Megias M, Emri Z, Freund TF, Gulyás AI. 2001. Total number and distribution of inhibitory and excitatory synapses on hippocampal CA1 pyramidal cells. *Neuroscience* 102:527–540.
- Migliore M. 1996. Modeling the attenuation and failure of action potentials in the dendrites of hippocampal neurons. *Biophys J* 71:2394–2403.
- Migliore M. 2003. On the integration of subthreshold inputs from perforant path and schaffer collaterals in hippocampal cal pyramidal neurons. *J Comput Neurosci* 14:185–192.
- Migliore M, Hoffman DA, Magee JC, Johnston D. 1999. Role of an A-type K^+ conductance in the back-propagation of action potentials in the dendrites of hippocampal pyramidal neurons. *J Comput Neurosci* 7:5–15.
- Nasuto SJ, Knape RM, Krichmar JL, Ascoli GA. 2001. Relation between neuronal morphology and electrophysiology in the kainate lesion model of Alzheimer's disease. *Neurocomputing* 38–40:1477–1487.
- Poirazi P, Brannon T, Mel BW. 2003. Arithmetic of subthreshold synaptic summation in a model CA1 pyramidal cell. *Neuron* 37:977–987.
- Poolos NP, Migliore M, Johnston D. 2002. Pharmacological upregulation of h-channels reduces the excitability of pyramidal neuron dendrites. *Nat Neurosci* 5:767–774.
- Pyapali GK, Sik A, Penttonen M, Buzsaki G, Turner DA. 1998. Dendritic properties of hippocampal CA1 pyramidal neurons in the rat: intracellular staining in vivo and in vitro. *J Comp Neurol* 391:335–352.
- Rall W. 1977. Core conductor theory and cable properties of neurons In: Kandel E, editor. *Handbook of physiology. The nervous system. Vol 1: Cellular biology of neurons*. Bethesda, MD: American Physiology Society. p 39–97.
- Spruston N, Johnston D. 1992. Perforated patch-clamp analysis of the passive membrane properties of three classes of hippocampal neurons. *J Neurophysiol* 67:508–529.
- Watanabe S, Hoffman DA, Migliore M, Johnston D. 2002. Dendritic K^+ channels contribute to spike-timing dependent long-term potentiation in hippocampal pyramidal neurons. *Proc Natl Acad Sci USA* 99:8366–8371.
- Wolf E, Birinyi A, Pomahazi S. 1995. A fast 3-dimensional neuronal tree reconstruction system that uses cubic polynomials to estimate dendritic curvature. *J Neurosci Methods* 63:137–145.